Clinical & Experimental Metastasis
https://doi.org/10.1007/s10585-023-10218-6

RESEARCH PAPER

Platycodin D represses β-catenin to suppress metastasis of cetuximab-treated *KRAS* wild-type colorectal cancer cells

Yongming Lv[1] · Wenhong Wang[1] · Yanfei Liu[2] · Ben Yi[2] · Tianhao Chu[2] · Zhiqiang Feng[2] · Jun Liu[3] · Xuehua Wan[4] · Yijia Wang[1]

Received: 8 February 2023 / Accepted: 5 June 2023

Abstract

Cetuximab, an epidermal growth factor receptor (EGFR) inhibitor, is extensively used for clinical therapy in KRAS wild-type colorectal cancer (CRC) patients. However, some patients still cannot get benefit from the therapy, because metastasis and resistance occur frequently after cetuximab treatment. New adjunctive therapy is urgently needed to suppress metastasis of cetuximab-treated CRC cells. In this study, we used two KRAS wild-type CRC cells, HT29 and CaCo2, to investigate whether platycodin D, a triterpenoid saponin isolated from Chinese medicinal herb Platycodon grandifloras, is able to suppress the metastasis of cetuximab-treated CRC. Label-free quantitative proteomics analyses showed that platycodin D but not cetuximab significantly inhibited expression of β-catenin in both CRC cells, and suggested that platycodin D counteracted the inhibition effect of cetuximab on cell adherence and functioned in repressing cell migration and invasion. Western blot results showed that single platycodin D treatment or combined platycodin D and cetuximab enhanced inhibition effects on expressions of key genes in Wnt/β-catenin signaling pathway, including β-catenin, c-Myc, Cyclin D1 and MMP-7, compared to single cetuximab treatment. Scratch wound-healing and transwell assays showed that platycodin D combined with cetuximab suppressed migration and invasion of CRC cells, respectively. Pulmonary metastasis model of HT29 and CaCo2 in nu/nu nude mice consistently showed that combined treatment using platycodin D and cetuximab inhibited metastasis significantly in vivo. Our findings provide a potential strategy to inhibit CRC metastasis during cetuximab therapy by addition of platycodin D.

Keywords Cetuximab · Platycodin D · Metastasis · β-catenin · Colorectal cancer

Introduction

Colorectal cancer (CRC) is the most common gastrointestinal malignancy with the third highest mortality and the fourth highest incidence worldwide, according to GLOBOCAN 2020 [1]. Although the diagnostic techniques and therapeutic approaches have advanced considerably over recent years, challenges of CRC treatment remain due to the resistance of CRC cells to treatment and consequent CRC metastasis. Cetuximab (CTX) is a monoclonal antibody targeting EGFR and is extensively used as the first-line therapy to treat *KRAS* wild-type CRC. Currently, although *KRAS* mutation is the only known determinant factor for CTX resistance, many reports indicate that overall survival of *KRAS* wild-type patients does not prolong with CTX treatment due to metastatic spread of tumor cells, e.g. resectable colorectal liver metastasis [2]. Metastasis and drug resistance substantially lead to the poor prognosis of CRC patients who have taken

Yongming Lv and Wenhong Wang contributed equally to this work and share first authorship.

✉ Xuehua Wan
xuehua.wan@hotmail.com

✉ Yijia Wang
yijiawang_1980@163.com

Yanfei Liu
lyanfei134@163.com

Jun Liu
junliu_sci@163.com

[1] Tianjin Union Medical Center, Nankai University, Tianjin, China

[2] School of Integrative Medicine, Tianjin University of Traditional Chinese Medicine, Tianjin, China

[3] The Fourth Central Hospital Affiliated to Nankai University, Tianjin, China

[4] TEDA Institute of Biological Sciences and Biotechnology, Nankai University, Tianjin, China

Published online: 16 June 2023

CTX therapy. As an EGFR tyrosine kinase inhibitor (TKI), CTX blocks downstream signaling pathways of EGFR tyrosine kinase. In these pathways, mutations of some key genes (such as BRAF and PI3KCA) cause CTX resistance [3]. Besides, Akt activation independent on EGFR phosphorylation contributes to drug resistance as well [4]. In addition, because mutation-mediated deactivation of β-catenin signaling pathways, such as Akt1/β-catenin and canonical Wnt signaling pathways, increased patient survival under EGFR TKI therapy, β-catenin mutations may play a pivotal role in resisting to metastasis in CRC patients who have taken CTX therapy [5–7]. Thus, exploring drugs that can function the same way as β-catenin mutations and deactivate β-catenin signaling pathway will help reduce metastasis caused by CTX treatment.β-catenin is the central component of the canonical Wnt signaling pathway, with an essential role in regulating cell fate determination, cell migration and polarity. Some mutations in the β-catenin phosphorylation sites stabilize β-catenin. As a consequence, these mutated non-phosphorylated β-catenin molecules translocate to the nucleus and continuously activate the expressions of Wnt target genes, such as c-Myc and cyclin D1 [8]. Mutations in β-catenin play a pro-tumorigenic role in promoting tumorigenesis in various types of human cancers including CRC [9]. Many researches showed that highly activated Wnt/β-catenin signaling pathway increases tumor metastasis and invasion. For example, the accumulation of β-catenin in cytoplasm upregulates MMP-7 expression to cause epithelial mesenchymal transformation (EMT) [10]. NCAPG, a cell cycle-associated condensin, upregulates β-catenin to facilitate EMT process in CRC cells [11]. Cinobufotalin inhibits EMT process via downregulating Wnt/β-catenin signaling pathway and then prevents the invasion and migration of hepatocellular carcinoma [12]. CTX combined with drugs that inhibit β-catenin can improve treatment effect by preventing metastasis and recurrence of certain types of cancer. For example, Dasatinib was used to sensitize *KRAS* mutant CRC cell lines to CTX through inhibition of β-catenin signaling pathways [13]. However, traditional Chinese medicines, which have relatively minor toxic side effects, have not been considered as adjunctive therapy for CTX treatment yet.

Traditional medicinal herbs and their natural compounds have been extensively used for treatment of cancer due to their advantages on low side effects and nontoxicity. Platycodin D (PD) is the major triterpene saponin extracted from the roots of Platycodon grandiflorum, which is a well-known traditional Chinese medicinal herb called Jiegeng in China [14]. Recent studies have shown that PD has various pharmacological potentials in treating human diseases, including tumor inhibition effect [15]. PD can be combined with another drug to enhance anti-tumor effect of the latter through regulation of Akt. For example, PD promoted the anti-cancer effects of sorafenib in Akt-positive and PTEN-negative prostate cancer cells through p-Akt ubiquitination [16]. PD suppressed bladder cancer through upregulation of miR-129-5p and inhibition of PI3K/Akt signaling pathways [17]. PD acts to show remarkable anti-tumor effects through complex mechanisms. Even if acting on Akt, PD has different regulation effects in different types of cancers. Until now, there still lacks research on understanding PD-mediated regulation of β-catenin signaling in any types of cancers.

In this work, we investigated whether PD can serve as an adjunctive therapy with CTX to suppress metastasis of *KRAS* wild-type CRC, by combining label-free quantitative proteomics analyses and in vitro and in vivo experiments. PD, CTX and combined drugs altered genome-wide protein expression patterns distinctly, and showed that PD but not CTX significantly inhibited expression of β-catenin in both *KRAS* wild-type CRC cells, HT29 and CaCo2. Gene Ontology enrichment analysis suggested that PD may counteract the inhibition effect of CTX on cell adherence and function in repressing cell migration and invasion. Western blot results and immunofluorescence staining results showed that PD downregulated expression and translocation of β-catenin in *KRAS* wild-type CRC cells. Both cell experiments and pulmonary metastasis model of HT29 and CaCo2 in nu/nu nude mice suggested that PD is able to repress metastasis of CRC in CTX therapy. Our findings open a way for establishing a novel strategy to improve prognosis outcome of late-stage CRC.

Results and discussion

CTX/PD suppressed CRC cell proliferation

To investigate the effects of CTX and PD on CRC cells, we performed CCK-8 assay to evaluate growth inhibition rates of CRC cells. The CCK-8 assay showed that CTX and PD both exhibited considerable inhibition effects on HT29 and CaCo2 cell proliferation (Fig. 1A–C). CTX showed more cytotoxicity on CaCo2 (IC50 = 1.3 μg/ml) than HT29 (IC50 = 22 μg/ml). This may be because HT29 has a mutated *BRAF* (V600E), which increases its resistance to CTX. Some studies also suggest that these two cell lines exhibit different intrinsic characteristics, e.g. expression patterns and mucin production/secretion abilities [18, 19]. PD showed similar cytotoxicity on both CaCo2 (IC50 = 34 μg/ml) and HT29 (IC50 = 36 μg/ml) cells. Furthermore, the combination treatment of CTX and PD showed no obvious synergy or antagonism, when they were administered to HT29 and CaCo2 cells. According to IC50, 0.26 μg/ml CTX and 6.8 μg/ml PD were used to treat CaCo2 cells, and 4.4 μg/ml CTX and 7.2 μg/ml PD were used to treat HT29 cells in label-free

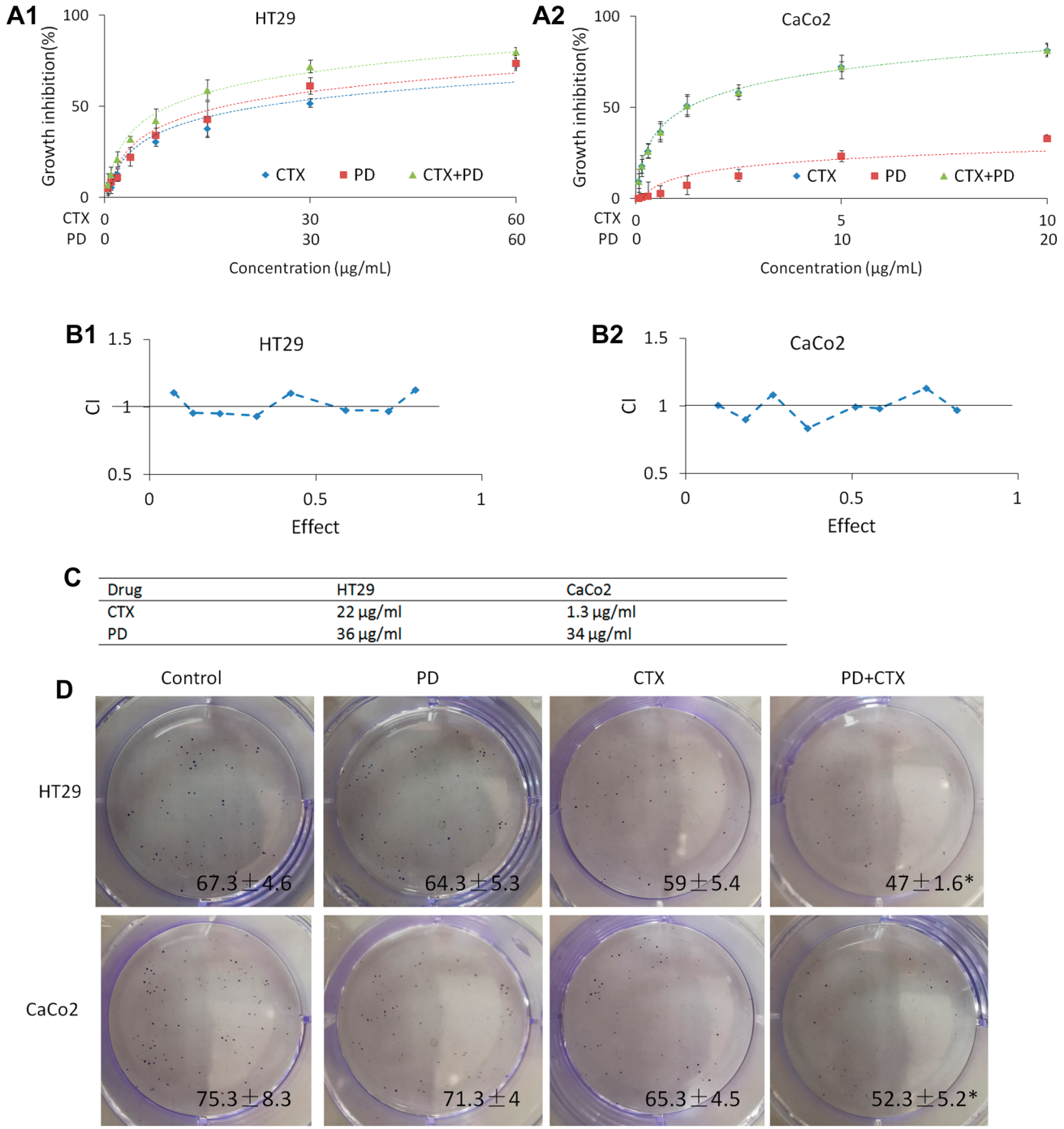

Fig. 1 CCK-8 assay and CalcuSyn analysis of drug effects on HT29 and CaCo2 cells. **A** CCK-8 assay evaluating drug effects on HT29 cells (A1) and CaCo2 cells (A2). The vertical axis represents growth inhibition rate, which is compared with untreated cells. The horizontal axis represents CTX and PD concentrations. **B** CalcuSyn analysis of the CCK-8 assay results. Combination index (CI) is calculated by calcusyn analysis based on the inhibition rates of different concentrations of CTX and PD. CI is roughly equal to 1, indicating that CTX and PD have addictive cytotoxicity. B1: HT29; B2: CaCo2. **C** IC50 of CTX and PD for the two cell lines, respectively. **D** The colony-formation assay evaluating drug effects on HT29 and CaCo2 cells. The data are displayed as mean of colony numbers ± SEM. 'Control' was compared with the other groups using one-way ANOVA. *P < 0.05 was calculated in these comparisons

quantitative proteomics analysis, scratch wound-healing, transwell invasion, western blot and immunocytochemistry assays. As shown in Fig. 1D, a colony formation assay was performed to further measure the antiproliferative effect of PD in combination with CTX under above conditions.

Consistent with the above data, the combination treatment of CTX and PD showed the highest inhibition rate as well.

PD/CTX/combined PD and CTX treatments altered global protein expression patterns distinctly

To predict the effects of PD and CTX on CRC and reveal involved key proteins and pathways, we next carried out label-free quantitative proteomics analyses of both HT29 and CaCo2 cells treated by PD, CTX, or combined PD and CTX. Principal component analysis of differential protein expression (DPE) confirmed that three types of treatments caused heteroproteinous global patterns of DPEs, and that two types of CRC cells responded to treatments distinctly (Fig. 2A). Hierarchically-clustered heatmap showed that each treatment condition was highly repeatable, and DPE patterns under PD and CTX treatment were closely clustered with those under PD treatment in both CRC cells (Fig. 2B). By contrast, DPE patterns under CTX treatment were closely clustered with those in the control condition in both CRC cells (Fig. 2B). Since CTX is a monoclonal antibody targeting EGFR, which inhibits the activation of EGF/EGFR-mediated downstream pathway, the effect of CTX on CRC cells may be relatively limited. By contrast, these data suggested that the effect of PD on CRC cells may be more complex. Thousands of proteins were differentially expressed in response to drugs in both HT29 and CaCo2 cells (Fig. 2C). Venn diagram based on DPEs with threefold changes consistently showed response variations in cell types and three treatments (Fig. 2D). Based on Top 10 enriched Gene Ontology (GO), either PD or CTX suppressed ATP metabolism and metal ion regulation in both CRC cells (Figure S1), suggesting that PD or CTX is capable of inhibiting Warburg effects in CRC cells. It has been reported that CTX reverses Warburg effects, which leads to inhibition of cancer cell metabolism [20]. Here, we for the first time found that PD showed a negative effect on Warburg effects as well. CTX additionally suppressed adherence abilities of both CRC cells (Figure S1), which may lead to tumor-cell dissociation from the primary lesion. But this suppression effect may also inhibit formation of metastasis and then cause anoikis. Consistently, it was shown that CTX treatment resulted in inhibition of cell adhesion, which accompanied with growth inhibition and reduced levels of cell adhesion molecules [21]. When PD and CTX were combined for treatment, both CRC cells decreased ATP metabolism and activities in response to peptide and drug (Figure S1). Activation of ATP metabolism promoted malignant progress of tumor, and ATP metabolism-related signature also regulated tumor immune microenvironment [22]. Our data suggested that CTX combined with PD also suppressed malignant progress of tumor via inhibition of ATP metabolism. In both CRC cells, expressions of 74 and 106 proteins were consistently up- and down-regulated, respectively, when PD treatments were compared to the control conditions and PD with CTX treatments were compared to CTX treatments (Fig. 3 and Figure S2). The expressions of proteins involved in fundamental cellular processes, such as ribosome proteins, vimentin, histone proteins and β-catenin, were downregulated in PD with CTX treatment (Fig. 3). Especially, because PD inhibited expressions of β-catenin (Fig. 3), which is a central regulator classified to most Top 10 GO groups (Figure S1), we speculated that PD may counteract the CTX-mediated inhibition effect on cell adherence through β-catenin signaling pathway and consequently play a pivotal role in repressing CRC cell migration and invasion.

PD/combined PD and CTX decreased the migration and invasion abilities of HT29 and CaCo2 cells

Based on the label-free quantitative proteomics results, we next carried out scratch wound-healing and transwell invasion assays to investigate whether PD decreased the migration and invasion abilities via inhibiting β-catenin in single treatment or combined treatment with CTX. Because CHIR-99021 (CHIR), a Wnt activator, was widely used to up-regulate wnt/β-catenin signaling pathway [9]. CHIR was then used to activate β-catenin in the following experiments. As shown in Figs. 4 and 5, PD and CTX treatments both decreased the migration and invasion abilities of HT29 and CaCo2 cells under single drug treatment condition. CHIR (for β-catenin activation) offset the inhibition effects of PD on the migration and invasion abilities of CRC cells, confirming that PD inhibits CRC cell migration and invasion through β-catenin signaling pathway. Combination of PD and CTX decreased the migration and invasion abilities of CRC cells dramatically, compared with single CTX treatment. By contrast, under CHIR combined treatment, PD cannot facilitate CTX to further decrease the migration and invasion abilities. Furthermore, 3 μM CHIR treatment showed almost no effect on proliferation of control or CTX treated cells (Figure S3).

PD inhibited β-catenin-mediated signaling pathway

As shown in Fig. 6, PD inhibited the expression levels of key proteins in β-catenin signaling pathway in HT29 and CaCo2 cells, whereas CTX showed no obvious effect on the expression levels of these proteins. PD also inhibited the expression levels of key proteins in β-catenin signaling pathway significantly when it was combined with CTX. As a Wnt/β-catenin activator, CHIR activated β-catenin signaling pathway and counteracted the effect of PD. Full length

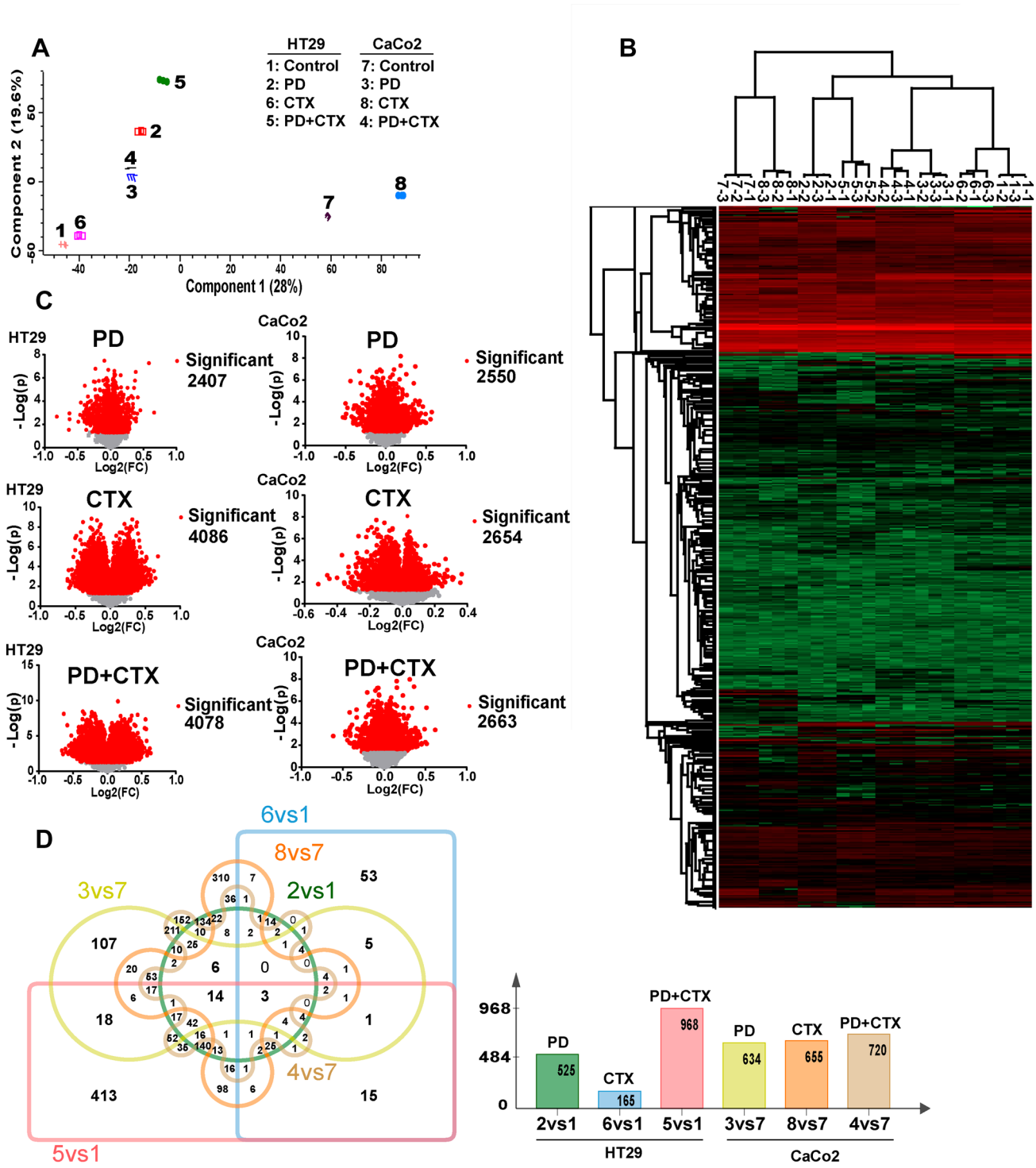

Fig. 2 Genome-wide protein expressions altered by PD/CTX/combined PD and CTX treatments. **A** Principal component analysis of differential protein expressions in PD/CTX/PD and CTX treated HT29 and CaCo2 cells. **B** Heatmap showing the changes in global protein expressions in PD/CTX/PD and CTX treated HT29 and CaCo2 cells. **C** Volcano plots of differential protein expressions in PD/CTX/PD and CTX treated HT29 and CaCo2 cells, compared to the control condition. **D** Venn diagram showing the numbers of differentially expressed proteins among conditions. 1: HT29 control; 2: PD-treated HT29; 6: CTX-treated HT29; 5: PD and CTX-treated HT29; 7: CaCo2 control; 3: PD-treated CaCo2; 8: CTX treated CaCo2; 4: PD and CTX-treated CaCo2

Fig. 3 Heatmap showing consistently down-regulated proteins by PD/combined PD and CTX treatments. The color scale bar represents the normalized Z scores of differentially expressed proteins. 1: HT29 control; 2: PD-treated HT29; 6: CTX-treated HT29; 5: PD and CTX-treated HT29; 7: CaCo2 control; 3: PD-treated CaCo2; 8: CTX treated CaCo2; 4: PD and CTX-treated CaCo2

western blots (all three independent experiments) of Fig. 6 is provided in Figure S4. Consistently, immunocytochemistry showed that PD inhibited translocation of β-catenin to nuclei, and CHIR counteracted this effect (Fig. 7).

PD combined with CTX reduced metastasis of HT29 and CaCo2 cells in vivo

To evaluate the effects of PD and CTX on reducing metastasis of HT29 and CaCo2 cells in vivo, HT29 and CaCo2 cells were injected to nu/nu nude mice via tail vein, to establish

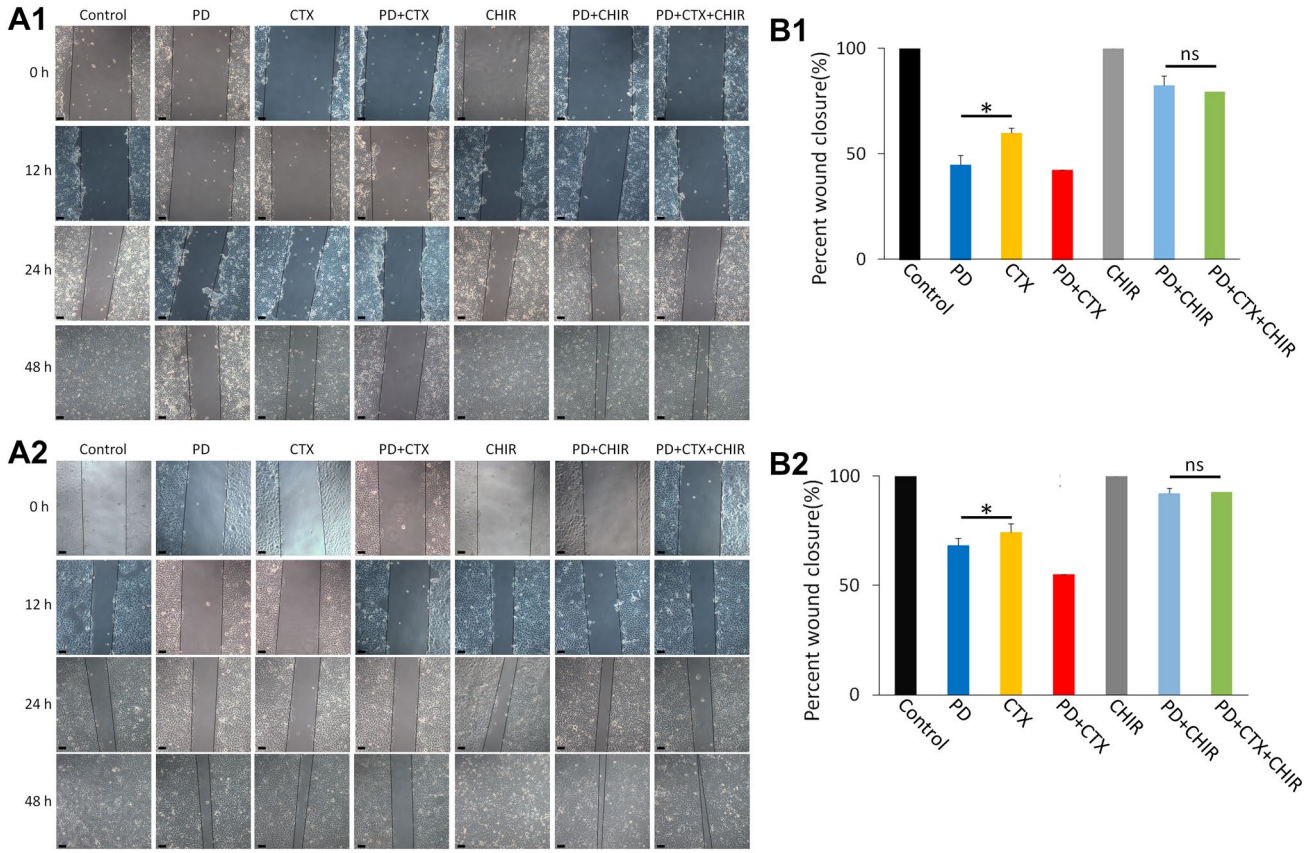

Fig. 4 Scratch wound-healing assay (original magnification 100×) showing effects of drugs on migration of CRC cells. **A** Migration images of scratch wound-healing assay. A1:HT29; A2: CaCo2. Scale bar: 50 μm (**B**) Bar plots of percent wound closure. B1: HT29; B2: CaCo2. 'CTX' was compared with 'PD and CTX' and 'PD and CHIR' was compared with 'PD, CTX and CHIR' using Student's t test. *: $P < 0.05$, *ns* no significance. 'PD and CTX', 'PD and CHIR' and 'PD, CTX and CHIR' represent the names of drugs in combination treatment

a mouse pulmonary metastasis model. Higher numbers of cancer nodules in the lungs of mice injected with HT29 and CaCo2 cells were found in the control groups than those in the treatment groups (Fig. 8). PD or CTX single treatment both decreased the numbers of cancer nodules slightly, suggesting that these two drugs had certain inhibition effect on metastasis. Combination treatment of PD and CTX dramatically decreased the numbers of cancer nodules, and increased integrity of alveolar structure, suggesting that the combined drugs showed synergistic effect on metastasis inhibition in vivo. These data indicated that PD or CTX may inhibit metastasis through their respective pathways. When CTX was used alone, the bypass pathway was not inhibited and CRC metastasis still occurred. When the two drugs were used at the same time, two independent pathways were both inhibited and the best inhibition effect on metastasis was achieved. Figure 8D showed the survival curves of all groups. All the mice ultimately died due to pulmonary metastasis. Mice in the control groups had the shortest survival time. Mice treated with PD or CTX had longer survival time than their untreated counterparts. The group with the combination treatment showed the best prognosis with the longest survival time. Furthermore, PD showed almost no side effects on liver, lung and kidney (Figure S5).

Bypass action role of PD in CTX resistance and CRC metastasis

The above data suggested that PD inhibited β-catenin-mediated signaling pathway and suppressed CRC metastasis. Besides, PI3K/Akt/mTOR and Ras/Raf/MAPK signaling pathways have been reported to be involved in CTX resistance and cancer cell migration. Some studies reported that PD regulated PI3K/Akt pathway, and PD up- or down-regulated p-Akt in different types of cancer [16, 17]. In addition, PD was shown to inhibit EGFR-mediated downstream MAPK signaling pathway in hepatocyte [23] and osteoclast differentiation [24]. To further understand the inhibitory mechanism of PD in CRC metastasis, we next compared the expression levels of key proteins in PI3K/Akt/mTOR

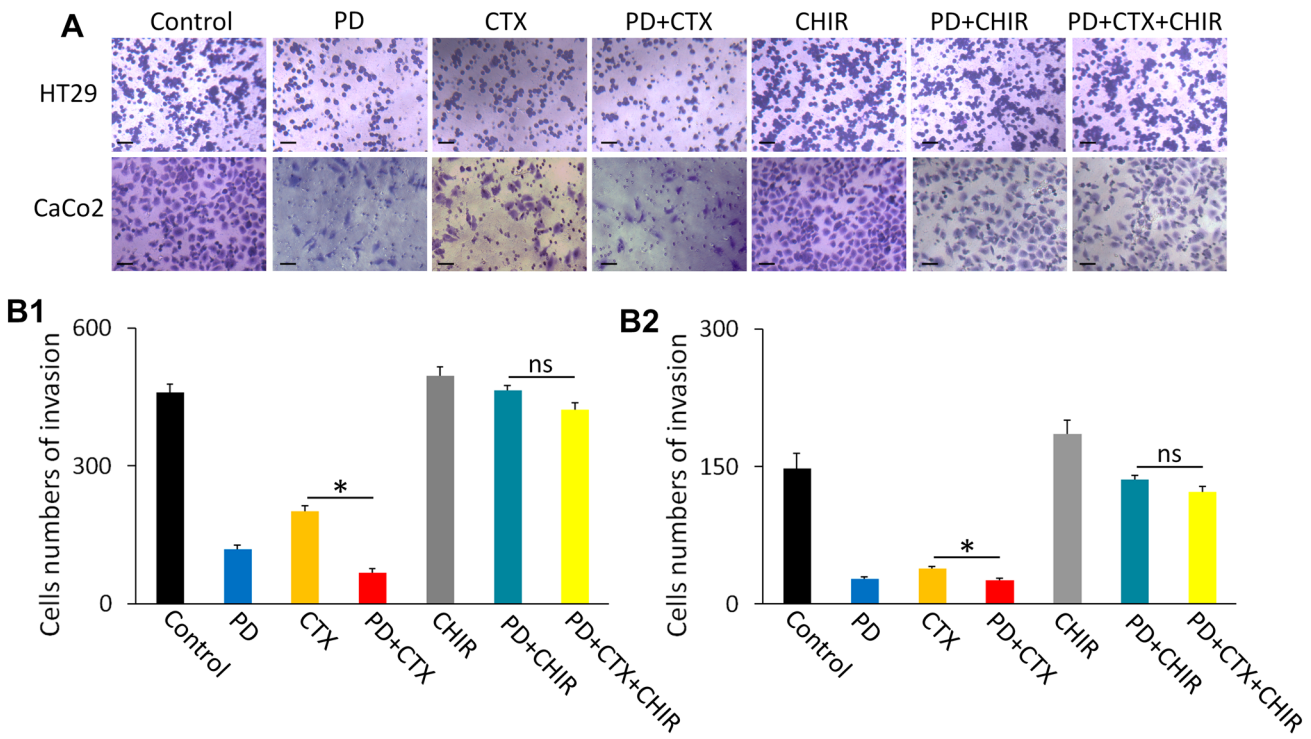

Fig. 5 Transwell assay showing effects of drugs on invasion of CRC cells. **A** Invasion images of Transwell assay. Scale bar: 50 μm (**B**) Bar plots of cell numbers of invasion. B1: HT29; B2: CaCo2. 'CTX' was compared with 'PD and CTX' and 'CTX and CHIR' was compared with 'PD, CTX and CHIR' using Student's t test. *: $P<0.05$, *ns* no significance. 'PD and CTX', 'PD and CHIR' and 'PD, CTX and CHIR' represent the names of drugs in combination treatment

and Ras/Raf/MAPK signaling pathways in CTX/PD/CTX and PD-treated HT29 or CaCo2 cells according to the results of quantitative proteomics analyses. PIK3C3 encodes the catalytic subunit of PI3K (K00922 in Fig. 11) that activates downstream kinase Akt [25]. Our data showed that in CaCo2 cells, CTX upregulated the expression level of PIK3C3, whereas PD inhibited the effect caused by CTX (Fig. 9A). AKT1S1 is a proline-rich substrate of Akt and inhibitor of mTOR [26]. PD significantly enhanced its expression and offset inhibition effect of CTX in CaCo2 cells, whereas PD and CTX showed no obvious regulation effects on AKT1S1 in HT29 cells (Fig. 9B). Some studies reported that sensitivity to anti-EGFR therapy is correlated with downregulation of phosphorylated Akt [27]. CTX did not down-regulate AKT1 in the two types of CRC cells (Fig. 9C). This may be because that CTX may inhibit p-Akt via disruption of EGF/EGFR binding reaction, however, pan-Akt expression may not be affected by CTX. mTOR is a central regulator of cell proliferation that is deregulated in cancer, and its phosphorylation contributes to CTX resistance [28]. mTOR expression was up-regulated by CTX (Fig. 9D), which may be due to the feedback mechanism of inhibition of mTOR phosphorylation by CTX [29]. PD treatment rescued this effect, suggesting that PD may modulate CRC resistance to CTX by inhibiting the expression of mTOR.

In Ras/Raf/MAPK pathway, RRAS and RRAS2 both encode GTPases that belong to R-Ras subfamily, of which mutations lead to metastatic cancer [30]. The treatments exhibited different effects on HT29 and CaCo2 cells (Fig. 9E, F), in which unknown mechanism need to be further investigated. In Ras/Raf/MAPK pathway, ARAF stabilizes polymer of BRAF and CRAF, and dimerization of ARAF promotes activation of MAPK [31]. Though CTX and PD both showed different regulation effects on ARAF, our results suggested that CTX did not inhibit ARAF effectively and PD suppressed expression of ARAF in CaCo2 cells (Fig. 9G). Moreover, MAPK1 (ERK2) [32] and MAPK9 (JNK2) [33] both promote cancer progress. CTX decreased the expression levels of these two proteins in CaCo2 but not those in HT29 cells (Fig. 9H, I). In theory, because CTX could down-regulate phosphorylation level of them by disrupting EGF/EGFR binding reaction, expression fluctuation of total proteins may be caused by other feedback mechanism. In addition, PD and combination treatment of PD and CTX both showed considerable down-regulation effects on MAPK1 expression. Taken together, PD regulated expressions of certain key proteins in both PI3K/Akt/mTOR and Ras/Raf/MAPK signaling pathways, and interfered with the effect of CTX on these two pathways, which may relieve CTX resistance.

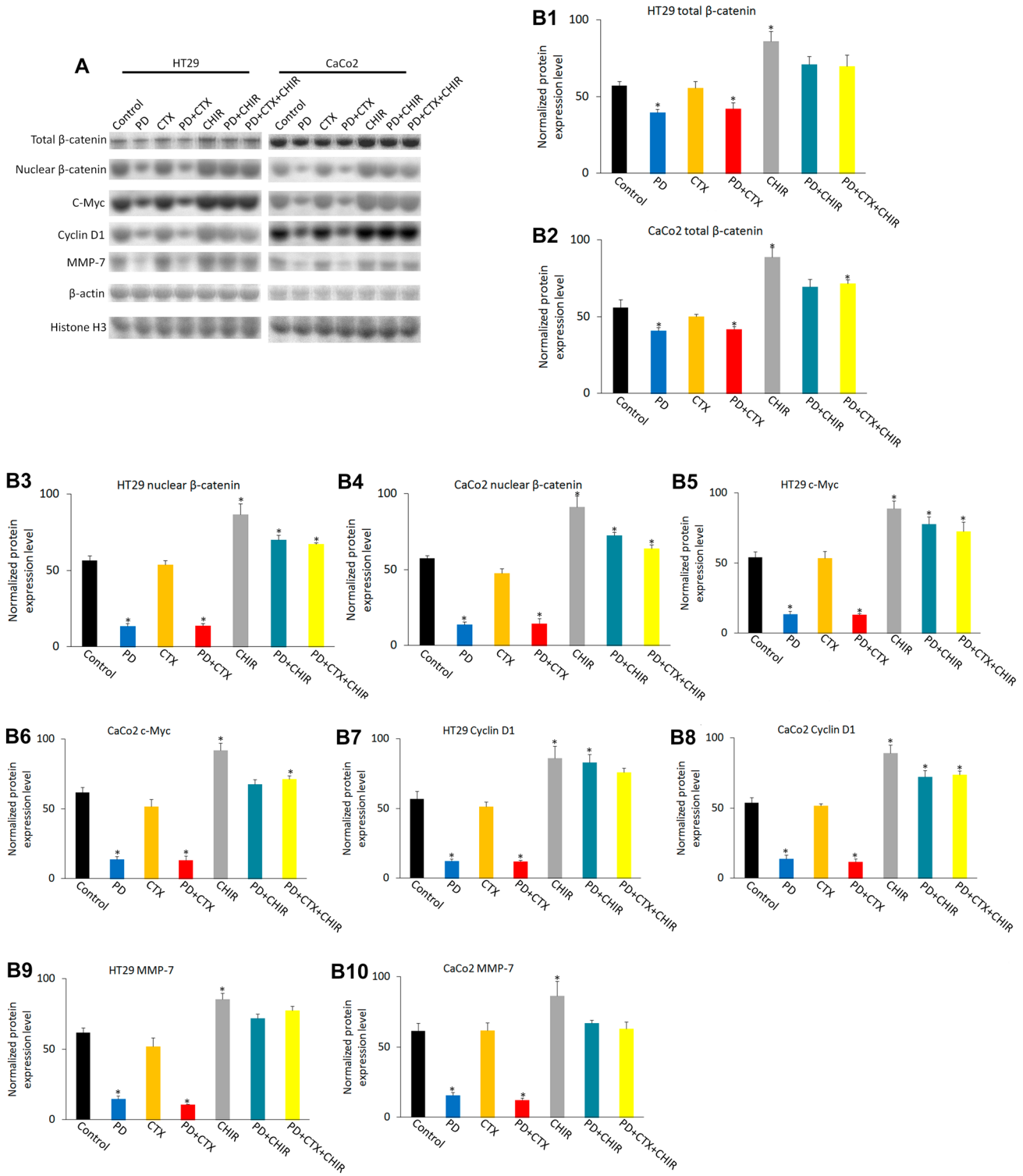

Fig. 6 Western blots showing the effect of co-treatment with PD and CTX on β-catenin-mediated signaling pathway in CRC cells. **A** Expression levels of the key proteins that are involved in β-catenin signaling pathway. The left column shows protein names, including total β-catenin, nuclear β-catenin, c-Myc, Cyclin D1, MMP-7, and two loading controls, β-actin and Histone H3. Western blots for all the proteins except nuclear β-catenin used β-actin as the loading controls. The top row shows two cell lines HT29 and CaCo2, and drug treatment with different combination. **B** Bar plots of densitometric analysis of three independent experiments. Protein expression levels are normalized by the loading controls. Columns show the mean ± SEM. Student's t test is used to analyze P values between groups. All groups are compared with the 'Control' group. *: $P < 0.05$

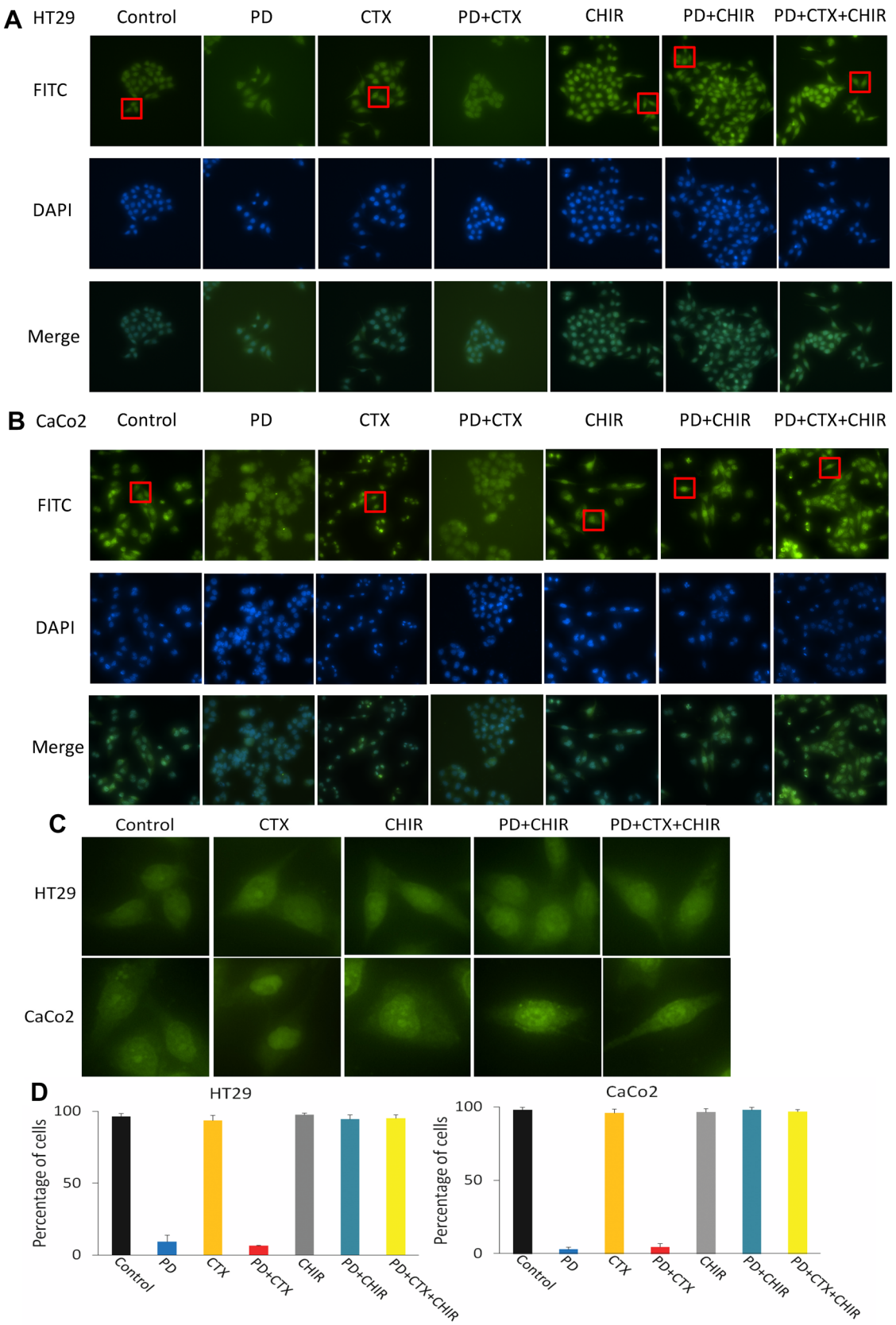

Fig. 7 Translocation of β-catenin in HT29 (**A**) and CaCo2 (**B**) cells with different drug treatments. Cells were immunostained with β-catenin antibody. Scale bar: 20 μm. **C** The area in red frame in part (**A**) and (**B**) was enlarged to exhibit nuclear translocation of β-catenin. **D** Percentage of cells with positive nuclear translocation in three independent experiments

CTX-mediated inhibition effects on EGFR downstream signaling pathways, such as Ras/Raf/MAPK and PI3K/Akt/mTOR, cause downregulation of migration and invasion in a certain degree, which is the mechanism of how CTX prevents CRC recurrence. Next, we examined PD-regulated key proteins involved in CRC cell migration and invasion according to the results of quantitative proteomics analyses. PD and combination treatment of PD and CTX increased expression levels of EPCAM (Fig. 10A), which may result in deregulated invasion [34]. PD and combination treatment of PD and CTX increased E-cadherin (CDH1) expression levels, and decreased N-cadherin (CDH2) expression levels (Fig. 10B, C), suggesting that PD could help CTX to inhibit migration and invasion via regulation conversion of E- to N-cadherin. Inhibition effect to vimentin (VIM) was also identified in PD and combination treatment of PD and CTX groups in these two cells (Fig. 10D), indicating inhibition effect of PD on epithelial-mesenchymal transition. These results further supported the above conclusions that PD combined with CTX suppressed CRC metastasis in vitro and in vivo (Fig. 11).

Materials and methods

Reagents and antibodies

All cell culture media, trypsin and antibiotics were purchased from Gibco (Grand Island, NY, USA), and fetal bovine serum (FBS) was purchased from HyClone (Logan, UT, USA). Rabbit anti-β-Catenin antibody (#8480, 1:1000 in western blot and 1:200 in Immunocytochemistry), rabbit anti-c-Myc antibody (#18583, 1:1000 in western blot), rabbit anti-Cyclin D1 antibody (#55506, 1:1000 in western blot), rabbit anti-MMP-7 antibody (#71031, 1:1000 in western blot), rabbit anti-β-Actin antibody (#4970, 1:1000 in western blot), rabbit anti-Histone H3 antibody (#4499, 1:2000 in western blot) were purchased from Cell Signaling Technology (Danvers, MA, USA). Goat anti-rabbit IgG-peroxidase (#DC03L, 1:20000 in western blot), FITC-conjugated goat anti-rabbit antibody (F0382, 1:80 in Immunocytochemistry) and DAPI were purchased from Sigma-Aldrich (St Louis, MO, USA). Nuclear and cytoplasmic protein extraction kit, CCK-8, CHIR-99021 (#SF2708) and PVDF membranes were purchased from Beyotime (Shanghai, China). ECL Plus substrate, RIPA lysis buffer and bicinchoninic acid reagents were purchased from CWBio (Beijing, China). 24-well Matrigel-coated chambers (6.5 mm in diameter, 8 μm pore-size, 100 μg/cm^2 Matrigel) were purchased from Corning (Tewksbury, MA, USA).

Cell lines

Human CRC cell lines, HT29 and CaCo2, were purchased from the Shanghai Institutes for Biological Sciences, Chinese Academy of Sciences (Shanghai, China). HT29 has wild-type KRAS and BRAF V600E mutant. CaCo2 has wild-type KRAS and BRAF. All cells were cultured in RPMI 1640 medium supplemented with 10% FBS, 100 μg/ml streptomycin, and 100 U/ml penicillin. According to the results of CCK-8 assay in Sect. PD/combined PD and CTX decreased the migration and invasion abilities of HT29 and CaCo2 cells, 0.2 IC50 of CTX, PD, and combined CTX and PD were used to treat cells for further analysis. Furthermore, 3 μM CHIR-99021 (CHIR), a GSK-3 inhibitor and Wnt/β-catenin activator [35], was used to treat cells to upregulate Wnt/β-catenin signaling pathway.

CTX and PD treatment

HT29 and CaCo2 were incubated in plate for 24 h and then treated with various concentrations of CTX and PD for another 48 h, in four different groups. (1) Control: cells without drug treatment; (2) CTX: cells treated with CTX alone for 48 h; (3) PD: cells treated with PD alone for 48 h; (4) CTX and PD: cells treated with a mixture of CTX and PD for 48 h. Cell viability was measured by CCK-8 assay. The rate of cell growth inhibition in each well was calculated by defining the absorption of control group as 100%. Measurements were performed in triplicate. Concentrations of CTX and PD for HT29 were both: 0.5, 0.95, 1.9, 3.75, 7.5, 15, 30, and 60 μg/ml. Concentrations of CTX for CaCo2 were: 0.075, 0.15, 0.3, 0.6, 1.25, 2.5, 5, and 10 μg/ml. Concentrations of PD for CaCo2 were: 0.15, 0.3, 0.6, 1.25, 2.5, 5, 10, and 20 μg/ml.

For colony formation assay, 400 cells per well were seeded in 6-well plates for 10 days. Then the cells were fixed in methanol for 15 min and stained with GIMSA application stain for 30 min, and imaged.

Sample preparation for label-free quantitative proteomics analyses

0.2 IC50 concentration of CTX, PD, and combined CTX and PD were used to treat HT29 and CaCo2. After treatment, proteins from three biological replications under each condition were extracted by liquid nitrogen grinding method. Next, 100 μl of SDT lysis buffer was added to each sample. The samples were incubated in boiling water bath for 3 min, ultrasonicated for 2 min, and then incubated in boiling water bath for 3 min. The samples were centrifuged to collect the supernatants. Protein quantification was performed using bicinchoninic acid (BCA) method. 300 μg of proteins from each sample were taken

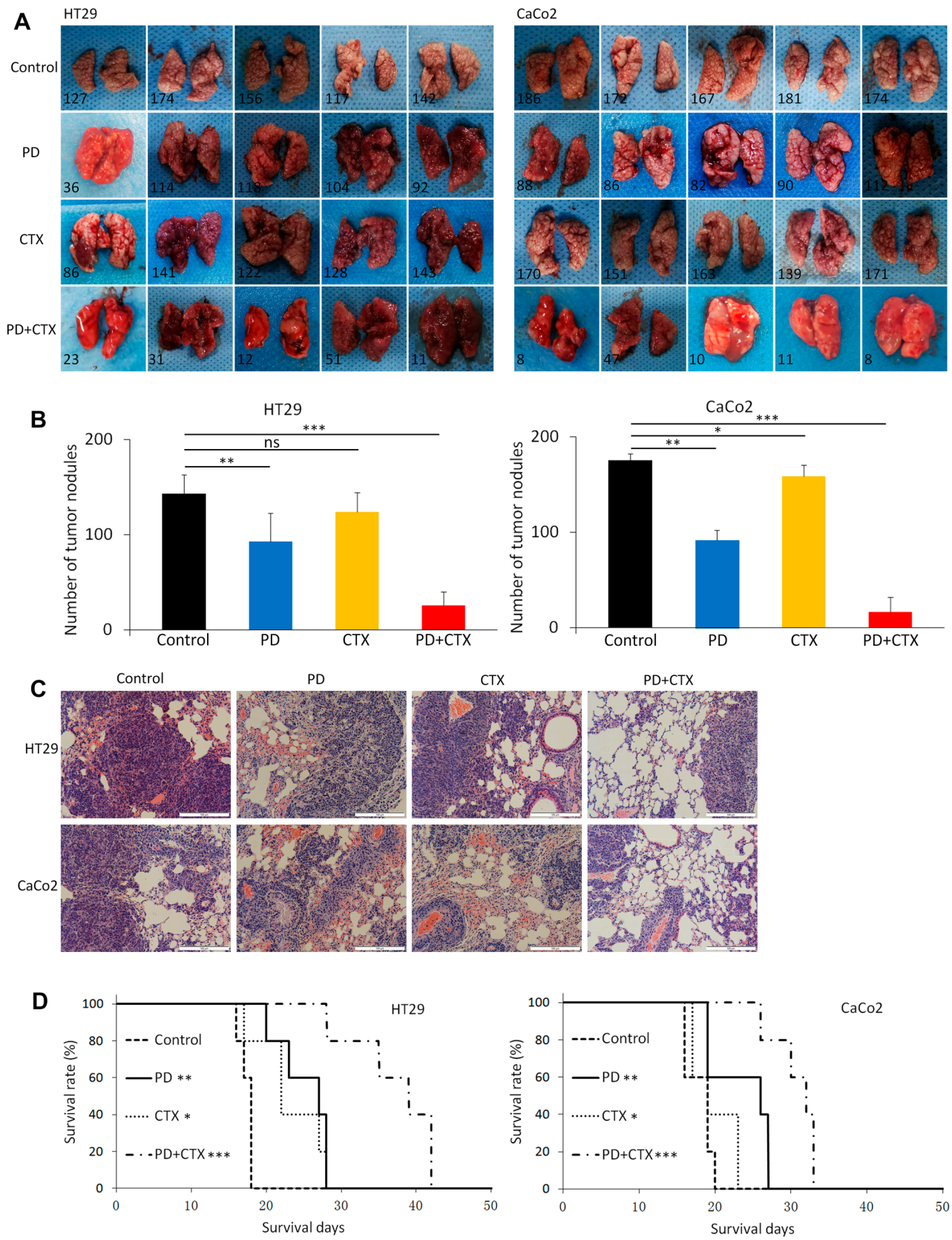
A
HT29
CaCo2
Control
PD
CTX
PD+CTX
127
174
156
117
142
186
172
167
181
174
36
114
118
104
92
88
86
82
90
112
86
141
122
128
143
170
151
163
139
171
23
31
12
51
11
8
47
10
11
8
B
HT29
CaCo2
Number of tumor nodules
200
100
0
***
ns
**
*
Control
PD
CTX
PD+CTX
C
Control
PD
CTX
PD+CTX
HT29
CaCo2
D
HT29
CaCo2
Survival rate (%)
100
80
60
40
20
0
Control
PD **
CTX *
PD+CTX ***
0
10
20
30
40
50
Survival days

◂**Fig. 8** Pulmonary metastases model and survival curves of mice. **A** Morphology of the lungs of each treatment group. Mice were sacrificed 14 days after injection of HT29 or CaCo2 cells via tail vein administration. Left labels showed drug treatment conditions. **B** Number of tumor nodules for each group. *P < 0.05, **P < 0.01, ***P < 0.001 represent various levels of difference between the indicated groups. **C** H&E staining of metastases lungs. Abundant cancer cells were found in lung tissue and destroyed alveolar structure in each group. Relatively complete alveolar structure can be found in 'PD + CTX' group, compared to those in other groups. Scale bar, 100 μm. **D** Survival curves of each group. Other groups were compared with control group. Each group has 5 mice. *: P < 0.05, **: P < 0.01, ***: P < 0.001, ns: no significance

for enzymatic hydrolysis in solution. Briefly, 1 M DTT was added to reach a final concentration of 100 mM. The samples were incubated in boiling water bath for 5 min, and cooled at room temperature. 1 M IAA (Indoleacetic acid) was added to reach a final concentration of 50 mM. The samples were kept away from light at room temperature for 20 min. Six volumes of acetone were added for precipitation. The samples were stored at − 20 °C for 4 h or overnight. The samples were centrifuged at 16,000 × g for 15 min. The pellets were washed with acetone twice, air dried and then dissolved in 8 M urea. The solution was diluted to 1 M urea using 50 mM NH_4HCO_3. An appropriate amount of trypsin was added and shaked at 37 °C overnight (16–18 h). After enzymatic hydrolysis, the peptides were desalted with C18 cartridge and lyophilized. The peptides were then re-dissolved in 0.1% trifluoroacetic acid and the concentration was determined for LC–MS/MS analysis.

LC–MS/MS analysis

An appropriate amount of peptides from each sample was used to perform chromatographic separation in a nano liter flow rate easy NLC 1200 chromatographic system (Thermo Scientific, USA). Buffer A contained 0.1% formic acid solution and buffer B contained 0.1% formic acid acetonitrile solution (80% for acetonitrile). The chromatographic column was in liquid equilibrium at 95% buffer A. The samples were injected to the trap column and then passed chromatography for gradient separation with a flow rate of 300 nL/min. The liquid phase gradient was set as follows: 0–2 min, the linear gradient of buffer B was from 5 to 8%; 2–90 min, the linear gradient of buffer B was from 8 to 23%; 90–100 min, the linear gradient of buffer B was from 23 to 40%; 100–108 min, the linear gradient of buffer B was from 40 to 100%; 108–120 min, buffer B was maintained at 100%. After peptides were separated, data-dependent acquisition mass spectrometry (DDA-MS) was performed on Q-Exactive HF-X mass spectrometer (Thermo Scientific, USA).

Label-free quantitative proteomics analyses at genome-wide scale

The LC–MS/MS data were searched against the Uniprot database (Species: Homo sapiens, protein numbers: 194324, accessed on 02/02/2021), using MaxQuant v1.6.0.16. The expression matrix was loaded to Perseus v1.6.15.0 for statistical and functional analyses. The data were filtered and processed according to the Perseus protocol (Tyanova and Cox). The plots of principal component analysis and hierarchical clustering of samples based on the correlation coefficients were performed using Perseus. Volcano plots were analyzed based on differentially expressed proteins (P < 0.05). Venn diagram plot was visualized based on differentially expressed proteins (P < 0.05) with fold changes either > 3 or < 1/3 via Jvenn program [36]. GO enrichment analysis of differentially expressed proteins were performed and visualized via ClusterProfiler v3.18.1 and R v4.0.3 [37]. Heatmaps were visualized using Perseus or R package pheatmap v1.0.12 [38].

Scratch wound-healing assay

The classical scratch wound-healing assay was used to determine the migratory ability of the cells as previously described [39]. Briefly, cells were cultured in six-well plates to form a monolayer. Then cells were serum-starved overnight, and an artificial scratch wound was created by a 10 μl pipette tip. At the same time, CTX, PD and CHIR were added to serum-free medium as single or combination to treat cells. Phase-contrast images of migration assay were captured from the time-lapse series at 0, 12, 24, and 48 h after scratching. Experiments were repeated independently in triplicate. The following equation was used to calculate percent wound closure: percent wound closure (%) = [1 − (Lt/L0)] × 100, where Lt represents width of scratch at time t and L0 represents initial width of scratch.

Cell invasion assay

24-well Matrigel-coated chambers were used in cell invasion assays as previously described [39]. Briefly, cells were grown until they reached subconfluent cell densities, and then serum-starved for 24 h. Cells were detached using trypsin, and 2×10^5 cells were added to the upper transwell chamber in 500 μl of serum-free medium. To the lower chamber, 750 μl of medium with 10% FBS was added to each well. All the experiments were repeated in triplicate. After 24 h incubation at 37 °C with 5% CO_2, cells that had not migrated were removed using a cotton swab and cells that had migrated were fixed with 4% paraformaldehyde and stained with 0.1% crystal violet for 30 min. Images of three different fields were captured for each membrane.

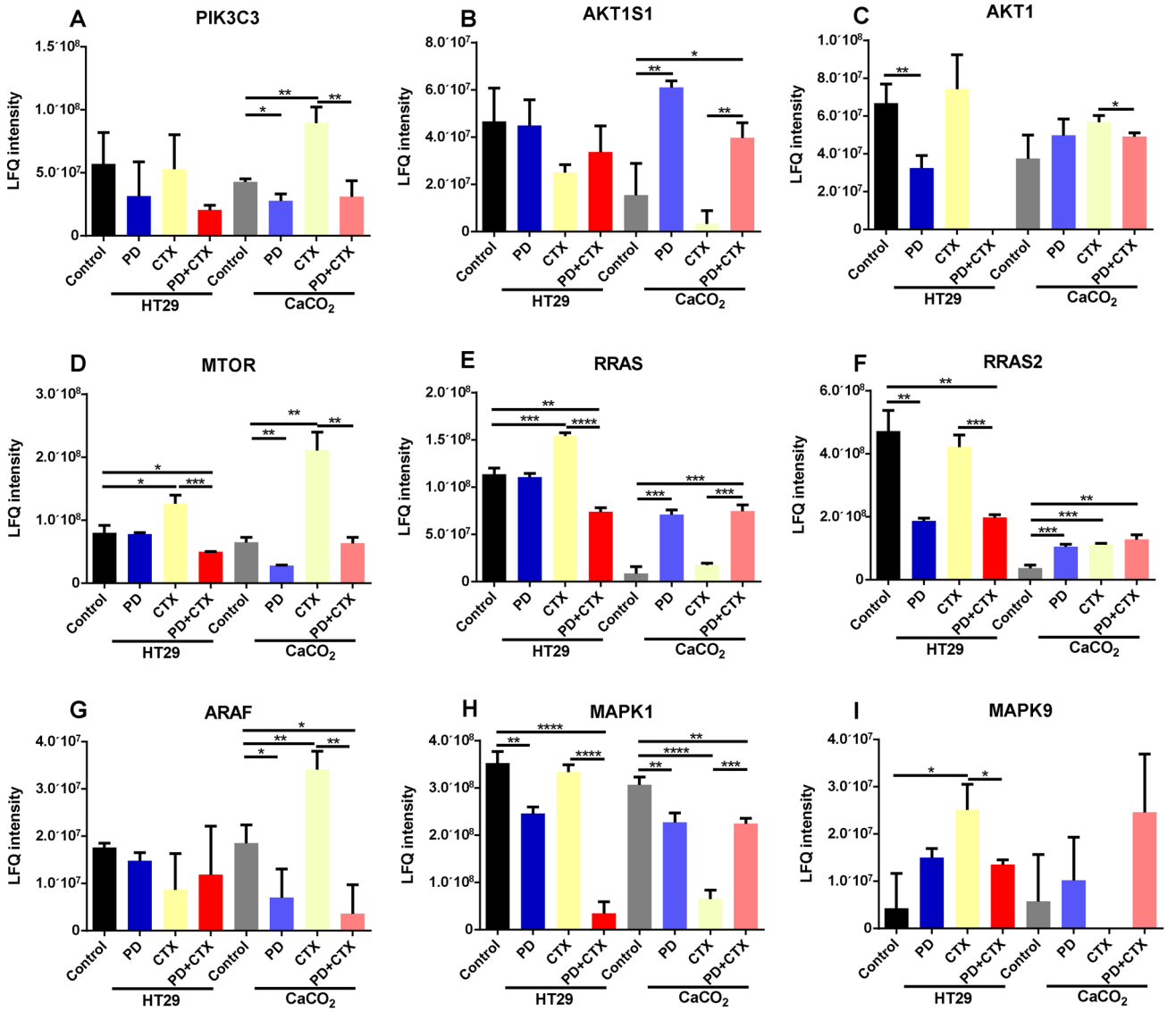

Fig. 9 Comparison of expression levels of key proteins in PI3K/Akt/mTOR and Ras/Raf/MAPK signaling pathways in CTX/PD/CTX and PD-treated HT29 or CaCo2 cells according to the results of quantitative proteomics analyses. 'LFQ intensity' represents label-free quantitative intensity. **A** Comparison of expression levels of PIK3C3. **B** Comparison of expression levels of AKT1S1. **C** Comparison of expression levels of AKT1. **D** Comparison of expression levels of mTOR. **E** Comparison of expression levels of RRAS. **F** Comparison of expression levels of RRAS2. **G** Comparison of expression levels of ARAF. **H** Comparison of expression levels of MAPK1. **I** Comparison of expression levels of MAPK9. *P < 0.05, **P < 0.01, ***P < 0.001, ****P < 0.001 (student's t test)

Western blotting

10^6 cells were lysed in 500 mL of RIPA lysis buffer supplemented with protease inhibitors for 20 min at 4 °C. The protein content in the sample lysate was quantitated by bicinchoninic acid reagents. Protein samples were then suspended in SDS loading buffer. After boiling, 10 µg of protein from each sample was separated by 10% SDS–polyacrylamide gel electrophoresis, and then transferred to Immobilon PVDF membranes. The membranes were probed with antibodies using standard techniques. Finally, the signals were visualized using ECL Plus and exposed film. Each assay was carried out in triplicate.

Immunocytochemistry analysis

Immunofluorescence staining was used to analyze β-catenin expression in cytoplasm and nucleus. The procedure was carried out as previously described [39]. In brief, cells were washed gently with PBS, fixed in 10% formalin at room temperature for 20 min, treated with 0.5% Triton X-100 for 5 min at 4 °C and then blocked with 5% normal

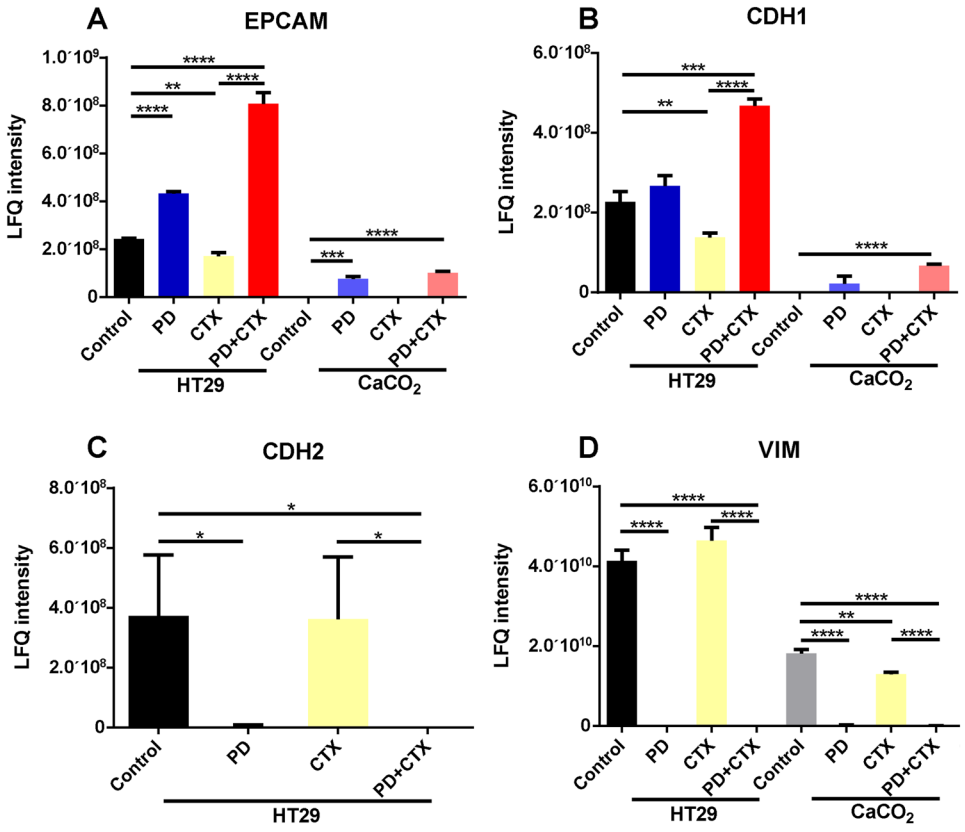

Fig. 10 Comparison of expression levels of key migration proteins in CTX/PD/CTX and PD-treated HT29 or CaCo2 cells according to the results of quantitative proteomics analyses. 'LFQ intensity' represents label-free quantitative intensity. **A** Comparison of expression levels of EPCAM. **B** Comparison of expression levels of CDH1. **C** Comparison of expression levels of CDH2. **D** Comparison of expression levels of VIM. $*P<0.05$, $**P<0.01$, $***P<0.001$, $****P<0.001$ (student's t test)

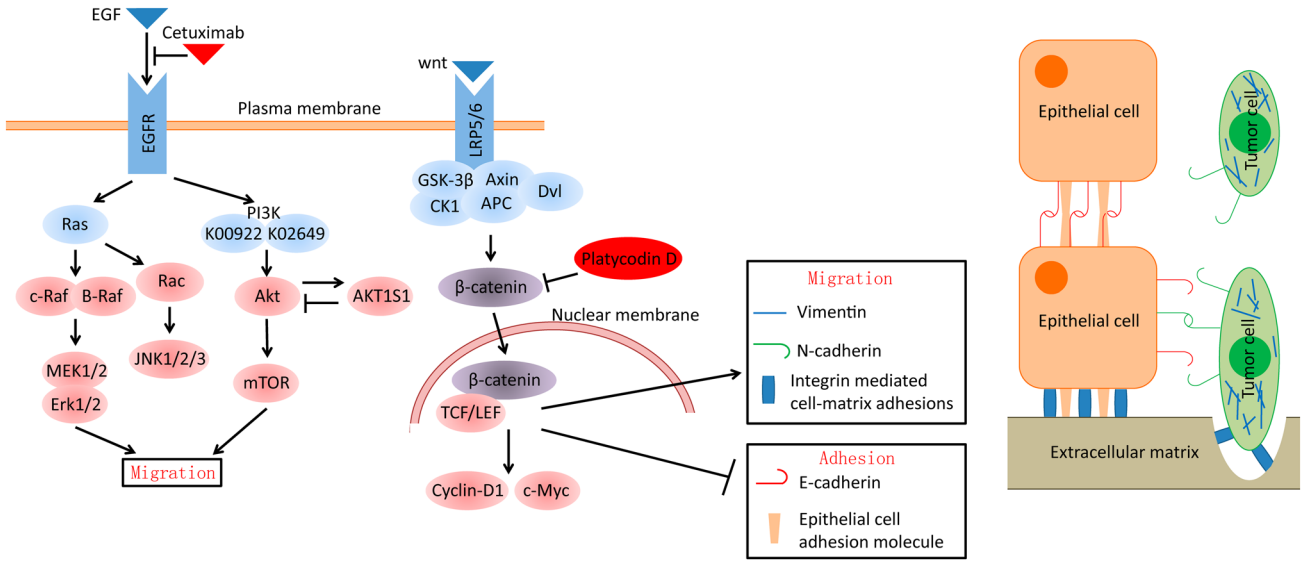

Fig. 11 Schematic diagram showing inhibitory roles of PD and CTX in the signaling pathways involved in CRC metastasis. CTX inhibits EGFR-mediated signaling pathways, whereas PD inhibits β-catenin-mediated signaling pathway. The co-treatment of PD and CTX inhibits CRC cell migration and enhances CRC cell adhesion ability, leading to suppressed metastasis of CRC

goat serum overnight at 4 °C. Slides were incubated with primary antibody for 1 h at 37 °C. After washing with PBS, the slides were incubated with FITC-conjugated secondary antibody and DAPI for 1 h at 37 °C. Subsequently, the slides were washed with PBS to remove antibody and then sealed. The slides were photographed immediately using a fluorescence microscope (Olympus, Tokyo, Japan).

In vivo pulmonary tumor metastasis model and treatment

HT29 and CaCo2 cells were trypsinized and injected into the tail vein of nu/nu nude mice (6-week-old, female, Institute of Medical Laboratory Animals, Chinese Academy of Medical Sciences) with a concentration of 2×10^5/0.2 ml to establish a model for metastatic lung tumors. PD and/or CTX were administered intraperitoneally after tumor cell injection. PD was dissolved in the solution of PEG400: Saline: Ethanol with a volume ratio 400:300:200. PD was administered at 2.5 mg/kg three times per week. CTX was administered at 8 mg/kg for HT29 and 0.4 mg/kg for CaCo2 three times per week. Mice were sacrificed 2 weeks after tumor cell injection, and tumor nodules on the surface of the lungs were counted. Survival times were compared among groups. All animal experiments complied with the National Institutes of Health Guide for the Care and Use of Laboratory Animals (NIH Publication No. 8023, revised 1978) and was approved by the Ethics Committee of Tianjin Union Medical Center.

Statistical analyses

Statistical analyses were performed using statistical analysis in Graphpad or Excel. The results were presented as mean ± standard error of mean (SEM). Statistical significance between two groups was analyzed using Student's t test. P value of < 0.05 was considered significant.

Conclusions

Latent metastasis of CRC commonly occurs and then may progress rapidly within a few months or years after first operation that is even followed by targeted therapy treatment. As an EGFR TKI, CTX is commonly used to treat CRC to prevent metastasis and recurrence after operation. Although the addition of CTX to chemotherapy improves the overall survival of patients with advanced inoperable metastatic disease in some studies, its usage in the perioperative setting in patients with operable disease confers a significant disadvantage in terms of overall survival [2]. The potential mechanism is not clearly understood yet. As an EGFR TKI, CTX can be combined with other drugs to inhibit EGFR or its downstream signaling pathways, leading to decreased resistance [40]. In this work, CCK-8 results showed that CTX/PD suppressed CRC cell proliferation. Label-free quantitative proteomics analyses showed that CTX/PD/CTX and PD altered protein expression patterns in CRC cells distinctly. Moreover, bioinformatics analysis suggested that key proteins in β-catenin-mediated pathway, which regulates cell migration and polarity, were downregulated by PD treatment. Western blot results further confirmed that PD used as single treatment or combined with CTX can downregulate β-catenin translocation, and c-Myc, Cyclin D1, MMP-7 expression levels, which may result in suppressing cell migration and invasion. Our scratch wound-healing and transwell invasion assays found that PD inhibited migration and invasion of cells, when it was administered with CTX, and β-catenin activator (CHIR) reversed this effect. In vivo experiments suggested that PD inhibited metastasis in pulmonary metastasis model of nude mice. Additionally, PD and CTX modulated the expression levels of certain key proteins in PI3K/Akt/mTOR and Ras/Raf/MAPK signaling pathways. To the best of our knowledge, this is the first time to show that PD inhibited metastasis of CTX treated *KRAS* wild-type CRC cells via inhibition of β-catenin (Fig. 11). Our findings provide a potential strategy by applying PD as an adjunctive therapy with CTX, to suppress CRC metastasis and improve CRC prognosis.

Supplementary Information The online version contains supplementary material available at https://doi.org/10.1007/s10585-023-10218-6.

Acknowledgements We thank Shanghai Bioprofile Technology Company, Ltd for providing technical help in label-free quantitative proteomics analyses.

Author Contributions Conceptualization, XW and YW; investigation, YL (Yongming Lv), WW, YL. (Yanfei Liu), BY, TC, ZF and JL; writing—original draft preparation, XW and YW; writing—review and editing, XW and YW All authors have read and agreed to the published version of the manuscript.

Funding This work was partially supported by the Natural Science Foundation of China Grant number 81972826 and 12174203.

Data availability statement All data were supported in manuscript and supplementary materials.

Declarations

Conflict of interest The authors have no conflict of interest.

Institutional review board statement All animal experiments complied with the National Institutes of Health Guide for the Care and Use of Laboratory Animals (NIH Publication No. 8023, revised 1978) and was approved by the Ethics Committee of Tianjin Union Medical Center.

References

1. Sung H, Ferlay J, Siegel RL, Laversanne M, Soerjomataram I, Jemal A et al (2021) Global Cancer Statistics 2020: GLOBOCAN estimates of incidence and mortality worldwide for 36 cancers in 185 Countries. CA Cancer J Clin 71:209–249. https://doi.org/10.3322/caac.21660
2. Bridgewater JA, Pugh SA, Maishman T, Eminton Z, Mellor J, Whitehead A et al (2020) Systemic chemotherapy with or without cetuximab in patients with resectable colorectal liver metastasis (New EPOC): long-term results of a multicentre, randomised, controlled, phase 3 trial. Lancet Oncol 21:398–411. https://doi.org/10.1016/S1470-2045(19)30798-3

3. Segelov E, Waring P, Desai J, Wilson K, Val G, Subotheni T et al (2016) ICECREAM: randomised phase II study of cetuximab alone or in combination with irinotecan in patients with metastatic colorectal cancer with either KRAS, NRAS, BRAF and PI3KCA wild type, or G13D mutated tumours. BMC Cancer 16:339. https://doi.org/10.1186/s12885-016-2389-8
4. Zaryouh H, Pauw ID, Baysal H, Pauwels P, Peeters M, Vermorken JB et al (2021) The role of Akt in acquired cetuximab resistant head and neck squamous cell carcinoma: an in vitro study on a novel combination strategy. Front Oncol 11:697967. https://doi.org/10.3389/fonc.2021.697967
5. Celikok GH, Sagirli PA, Ulbegi GA, Can A (2021) Identification of AKT1/β-catenin mutations conferring cetuximab and chemotherapeutic drug resistance in colorectal cancer treatment. Oncol Lett 21:209. https://doi.org/10.3892/ol.2021.12470
6. Casas-Selves M (2012) Tankyrase and the canonical Wnt pathway protect lung cancer cells from EGFR inhibition. Cancer Res 72:4154–4164. https://doi.org/10.1158/0008-5472.CAN-11-2848
7. Lu Y, Zhao X, Liu Q, Li C, Graves-Deal R, Cao Z et al (2017) lncRNA MIR100HG-derived miR-100 and miR-125b mediate cetuximab resistance via Wnt/β-catenin signaling. Nat Med 23:1331–1341. https://doi.org/10.1038/nm.4424
8. Hagen T, Vidal-Puig A (2002) Characterisation of the phosphorylation of beta-catenin at the GSK-3 priming site Ser45. Biochem Biophys Res Commun 294:324–328. https://doi.org/10.1016/S0006-291X(02)00485-0
9. Zhang Q, Yang X, Wu J, Ye S, Gong J, Cheng W et al (2023) Reprogramming of palmitic acid induced by dephosphorylation of ACOX1 promotes β-catenin palmitoylation to drive colorectal cancer progression. Cell Discov 9:26. https://doi.org/10.1038/s41421-022-00515-x
10. Iwai S, Yonekawa A, Harada C, Hamada M, Katagiri W, Nakazawa M (2010) Involvement of the Wnt-b-catenin pathway in invasion and migration of oral squamous carcinoma cells. Int J Oncol 37:1095–1103. https://doi.org/10.3892/ijo_00000761
11. Shi Y, Ge C, Fang D, Wei W, Li L, Wei Q et al (2022) NCAPG facilitates colorectal cancer cell proliferation, migration, invasion and epithelial-mesenchymal transition by activating the Wnt/β-catenin signaling pathway. Cancer Cell Int 22:119. https://doi.org/10.1186/s12935-022-02538-6
12. Li W, Pei S, Zhang X, Qi D, Zhang W, Dou Y et al (2022) Cinobufotalin inhibits the epithelial-mesenchymal transition of hepatocellular carcinoma cells through down-regulate β-catenin in vitro and in vivo. Eur J Pharmacol. https://doi.org/10.1016/j.ejphar.2022.174886
13. Dunn EF, Iida M, Myers RA, Campbell DA, Hintz KA, Armstrong EA et al (2011) Dasatinib sensitizes KRAS mutant colorectal tumors to cetuximab. Oncogene 30:561–574. https://doi.org/10.1038/onc.2010.430
14. Li W, Liu Y, Wang Z, Han Y, Tian YH, Zhang GS et al (2015) Platycodin D isolated from the aerial parts of Platycodon grandiflorum protects alcohol-induced liver injury in mice. Food Funct 6:1418–1427. https://doi.org/10.1039/c5fo00094g
15. Nyakudya E, Jeong JH, Lee NK, Jeong YS (2014) Platycosides from the roots of platycodon grandiflorum and their health benefits. Prev Nutr Food Sci 19:59–68. https://doi.org/10.3746/pnf.2014.19.2.059
16. Lu Z, Song W, Zhang Y, Wu C, Zhu M, Wang H et al (2021) Combined anti-cancer effects of Platycodin D and Sorafenib on androgen-independent and PTEN-deficient prostate cancer. Front Oncol 11:648985
17. Chen D, Chen T, Guo Y, Wang C, Dong L, Lu C (2021) Suppressive effect of platycodin D on bladder cancer through microRNA-129–5p-mediated PABPC1/PI3K/AKT axis inactivation. Braz J Med Biol Res 54:e10222. https://doi.org/10.1590/1414-431X202010222
18. Bertrand V, Couturier-Turpin MH, Louvel A, Panis Y, Couturier D (1999) Relation between cytogenetic characteristics of two human colonic adenocarcinoma cell lines and their ability to grow locally or metastasize or both: an experimental study in the nude mouse. Cancer Genet Cytogenet 113:36–44. https://doi.org/10.1016/s0165-4608(98)00194-0
19. Lian P, Braber S, Varasteh S, Wichers HJ, Folkerts G (2011) Hypoxia and heat stress affect epithelial integrity in a Caco-2/HT-29 co-culture. Sci Rep 11:13186. https://doi.org/10.1038/s41598-021-92574-5
20. Luo J, Hong Y, Lu Y, Qiu S, Chaganty B, Zhang L et al (2017) Acetyl-CoA carboxylase rewires cancer metabolism to allow cancer cells to survive inhibition of the Warburg effect by cetuximab. Cancer Lett 384:39–49. https://doi.org/10.1016/j.canlet.2016.09.020
21. El Hallal R, Lyu N, Wang Y (2021) Effect of cetuximab-conjugated gold nanoparticles on the cytotoxicity and phenotypic evolution of colorectal cancer cells. Molecules 26:567. https://doi.org/10.3390/molecules26030567
22. Huang R, Li G, Wang Z, Hu H, Zeng F, Zhang K et al (2020) Identification of an ATP metabolism-related signature associated with prognosis and immune microenvironment in gliomas. Cancer Sci 111:2325–2335. https://doi.org/10.1111/cas.14484
23. Fu C, Liu Y, Leng J, Zhang J, He Y, Chen C et al (2018) Platycodin D protects acetaminophen-induced hepatotoxicity by inhibiting hepatocyte MAPK pathway and apoptosis in C57BL/6J mice. Biomed Pharmacother 107:867–877. https://doi.org/10.1016/j.biopha.2018.08.082
24. Choi J, Han Y, Kim Y, Jin S, Lee G, Jeong H et al (2017) Platycodin D inhibits osteoclastogenesis by repressing the NFATc1 and MAPK signaling pathway. J Cell Biochem 118:860–868. https://doi.org/10.1002/jcb.25763
25. Zhang Y, Hu B, Li Y, Deng T, Xu Y, Lei J et al (2020) Binding of Avibirnavirus VP3 to the PIK3C3-PDPK1 complex inhibits autophagy by activating the AKT-MTOR pathway. Autophagy 16:1697–1710. https://doi.org/10.1080/15548627.2019.1704118
26. Choi M (2015) Inactivating frameshift mutation of AKT1S1, an mTOR inhibitory gene, in colorectal cancers. Scand J Gastroenterol 50:503–504. https://doi.org/10.3109/00365521.2014.971341
27. Amato VD, Rosa R, Amato CD, Formisano L, Marciano R, Nappi L et al (2014) The dual PI3K/mTOR inhibitor PKI-587 enhances sensitivity to cetuximab in EGFR-resistant human head and neck cancer models. Br J Cancer 110:2887–2895. https://doi.org/10.1038/bjc.2014.241
28. Izumi H, Wang Z, Goto Y, Ando T, Wu X, Zhang X et al (2020) Pathway-specific genome editing of PI3K/mTOR tumor suppressor genes reveals that PTEN loss contributes to cetuximab resistance in head and neck cancer. Mol Cancer Ther 19:1562–1571. https://doi.org/10.1158/1535-7163.MCT-19-1036
29. Alalem M, Ray A, Ray BK (2016) Metformin induces degradation of mTOR protein in breast cancer cells. Cancer Med 5:3194–3204. https://doi.org/10.1002/cam4.896
30. Cubelos B (2013) R-RAS2 overexpression in tumors of the human central nervous system. Mol Cancer 12:127. https://doi.org/10.1186/1476-4598-12-127
31. Su W, Mukherjee R, Yaeger R, Son J, Xu J, Na N et al (2022) ARAF protein kinase activates RAS by antagonizing its binding to RASGAP NF1. Mol Cell 82:2443–57.e7. https://doi.org/10.1016/j.molcel.2022.04.034
32. Wang H, Ke J, Guo Q, Nampoukime KB, Yang P, Ma K (2018) Long non-coding RNA CRNDE promotes the proliferation, migration and invasion of hepatocellular carcinoma cells through miR-217/MAPK1 axis. J Cell Mol Med 22:5862–5876. https://doi.org/10.1111/jcmm.13856
33. Yang R, Jiheng Xu, Hua X et al (2020) Overexpressed miR-200a promotes bladder cancer invasion through direct regulating Dicer/

miR-16/JNK2/MMP-2 axis. Oncogene 39(9):1983–1996. https://doi.org/10.1038/s41388-019-1120-z
34. Sankpal NV, Brown TC, Fleming TP, Herndon JM, Amaravati AA, Loynd AN et al (2021) Cancer-associated mutations reveal a novel role for EpCAM as an inhibitor of cathepsin-L and tumor cell invasion. BMC Cancer 21:541. https://doi.org/10.1186/s12885-021-08239-z
35. Zhao A, Qin H, Sun M, Tang M, Mei J, Ma K et al (2021) Chemical conversion of human epidermal stem cells into intestinal goblet cells for modeling mucus-microbe interaction and therapy. Sci Adv 7:eabb2213. https://doi.org/10.1126/sciadv.abb2213
36. Bardou P, Mariette J, Escudié F, Djemiel C, Klopp C (2014) jvenn: an interactive Venn diagram viewer. BMC Bioinform 15:293. https://doi.org/10.1186/1471-2105-15-293
37. Tianzhi W, Erqiang H, Shuangbin X, Meijun C, Pingfan G, Zehan D et al (2021) clusterProfiler 4.0: a universal enrichment tool for interpreting omics data. Innovation (Camb) 2:100141. https://doi.org/10.1016/j.xinn.2021.100141
38. Raivo K (2019) pheatmap: Pretty Heatmaps. R package version 1.0.12. https://CRAN.R-project.org/package=pheatmap.
39. Shi G, Zheng X, Wu X, Wang S, Wang Y, Xing F (2019) All-trans retinoic acid reverses epithelial-mesenchymal transition in paclitaxel-resistant cells by inhibiting nuclear factor kappa B and upregulating gap junctions. Cancer Sci 110:379–388. https://doi.org/10.1111/cas.13855
40. Wang Y, Wang W, Wu X, Li C, Huang Y, Zhou H et al (2020) Resveratrol sensitizes colorectal cancer cells to cetuximab by connexin 43 upregulation-induced Akt inhibition. Front Oncol 10:383. https://doi.org/10.3389/fonc.2020.00383